Indian Journal of Pure & Applied Physics
Vol. 54, April 2016, pp. 227-235

Structural, anisotropic and thermodynamic properties of boron carbide: First principles calculations

Qingyang Fan[a], Qun Wei[b]*, Changchun Chai[a], Haiyan Yan[c], Meiguang Zhang[d], Zixia Zhang[a], Junqin Zhang[a] & Dongyun Zhang[e]

[a]State Key Discipline Laboratory of Wide BandGap Semiconductor Technology, School of Microelectronics, Xidian University, Xi'an 710071, China
[b]School of Physics and Optoelectronic Engineering, Xidian University, Xi'an 710071, P R China
[c]College of Chemistry and Chemical Engineering, Baoji University of Arts and Sciences, Baoji 721013, China
[d]Department of Physics and Information Technology, Baoji University of Arts and Science, Baoji 721016, China
[e]National Supercomputing Center in Shenzhen, Shenzhen 518055, P R China

Received 14 March 2015; revised 24 November 2015; accepted 7 January 2016

The structural, mechanical, electronic properties of the potentially superhard $P4_2$/mnm-BC have been investigated by using the density functional theory with the ultrasoft psedopotential scheme in the frame of the generalized gradient approximation and the local density approximation. The elastic constants, bulk modulus, shear modulus, Young's modulus, *B*/*G* ratio and Poisson's ratio for BC at various pressures have been investigated. The elastic anisotropy under pressure from 0 GPa to 100 GPa has been studied. The elastic anisotropy of Young's modulus, shear modulus, and Poisson's ratio show that $P4_2$/mnm-BC exhibits a large anisotropy and the elastic anisotropy increases with increasing pressure. Electronic structure studies show that $P4_2$/mnm-BC is a conductor. Using the quasi-harmonic Debye model, the thermodynamic properties of $P4_2$/mnm-BC have also been investigated. The variation of the thermal expansion, isothermal bulk modulus, Debye temperature, Grüneisen parameter, and heat capacity with pressure and temperature have been obtained systematically.

Keywords: *Ab-initio* calculations, Elastic properties, Electronic structure, Thermodynamic properties

1 Introduction

Diamond, with its extraordinary high hardness, has always been a very attractive material for many specific applications. But it is exceptionally weak for steel cutting and is burned to carbon dioxide at 800-900 °C in air. Boron doped diamond has attracted more interest because of its high hardness, high chemical stability, and superconductivity with relatively high transition temperature[1-6]. Solozhenko *et al.*[2] reported that the c-BC_5 solid solution, synthesized at a pressure of 24 GPa and temperature of 2200 K, has load-invariant hardness of about 71 GPa, with high thermal stability up to 1900 K. The boron carbide has many advantages over diamond, performing with high oxidation resistance and exhibits interesting electrical properties rather than insulator[7-10]. Experimental attempts have been made intensively to synthesize those compounds[2,10-12], including BC_2, BC_3, BC_5, and BC_7 . Boron carbide, often incorrectly denoted as B_4C, belongs to the structure group of α-rhombohedral boron within the icosahedral boron-rich solids. Its homogeneity range extends from $B_{4.3}C$ at the carbon-rich limit to $B_{11}C$ at the boron-rich limit. The compound B_4C does not exist. This was demonstrated by Schwetz and Karduck[13] for the first time, and has since been confirmed by numerous other experimental investigations. According to theoretical calculations[14-16], the compound $B_{13}C_2$ with the hypothetical structure formula B_{12} (C–B–C) is metallic in contrast to the real semiconducting boron carbide, is the energetically most favourable structure. The Fermi level is pinned within these split-off valence states up to very high temperatures, hence essentially determining the *p*-type semiconducting behaviour[17,18]. A superhard[19] B_4C_4 phase has been predicted using the particle swarm optimization algorithm. The structural stability of B_4C_4 has been confirmed from the calculations of the elastic constants and phonon frequency. The analysis of the electron structure of the predicted B_4C_4 indicates that it is an insulator, and the calculated theoretical Vickers hardness of B_4C_4 is 51.54 GPa, indicating that

*Corresponding author (E-mail: weiaqun@163.com)

B_4C_4 is a potential superhard material. The detailed ideal strength calculations show that B_4C_4 is easier to be subjected to shear deformation than tensile deformation[20]. By using crystal structure prediction technique, Wang *et al.*[21] theoretically predicted that a new $P4_2/mnm$ phase for BC is mechanically and dynamically stable. In the present work, the structural and mechanical properties of BC, including the elastic constants and the elastic anisotropy, have been systematically investigated. In addition, the aim of the present work is to study the pressure and temperature effects on the thermodynamic properties of BC using the first principles calculations. The thermodynamic properties, such as heat capacity, thermal expansion, isothermal bulk modulus, Grüneisen parameters, and Debye temperature have been investigated by the quasi-harmonic Debye model.

2 Theoretical Method

Calculations were performed using density functional theory[22,23] (DFT) with the generalized gradient approximation (GGA) parameterized by Perdew, Burke and Ernzerrof[24] (PBE) and the local density approximation[25,26] (LDA) as implemented in the CASTEP code[27] . The total energy convergence tests showed that convergence to within 1 meV/atom was achieved with the above calculation parameters. In the structure calculation, a plane-wave basis set with energy cut-off 460 eV is used. The Vanderbilt ultrasoft pseudopotential was used in the present work. The proper k-point grid (9×9×14) in the Brillouin zone is obtained with respect to the Monkhorst–Pack method [28]. All forces on atoms were converged to less than 0.001 eV/atom for the geometry relaxation and all the components of the Hellmann-Feynman stress tensor were reduced to the order of 0.01 GPa at the given pressure. The Broyden-Fletcher-Goldfarb-Shanno[29] (BFGS) minimization scheme was used in geometry optimization. The self-consistent convergence of the total energy is 5×10^{-6} eV/atom; the maximum force on the atom is 0.01eV/Å and the maximum ionic displacement is within 5×10^{-4} Å.

It is well known that the anisotropy of elasticity is an important implication in engineering science and crystal physics. So we keep on investigating the anisotropy of $P4_2/mnm$-BC. The stiffness tensor expresses the stress tensor in terms of the strain tensor: $\sigma_{ij} = C_{ijkl}\,\varepsilon_{kl}$. C_{ijkl} is elastic stiffness constant. The compliance tensor is the inverse of the stiffness tensor and interprets the strain tensor in terms of the stress tensor: $\varepsilon_{ij} = S_{ijkl}\,\sigma_{kl}$. The S_{ijkl} is the elastic compliance constant. Young's modulus is defined as the ratio of normal stress to linear normal strain (both in the direction of applied load). The shear modulus is defined as the ratio of shear stress to linear shear strain. Poisson's ratio is defined as the ratio of transverse strain (normal to the applied load) to axial strain (in the direction of the applied load).

A fourth order tensor transforms in a new basis set following the rule:

$$S'_{\alpha\beta\gamma\delta} = r_{\alpha i} r_{\beta j} r_{\gamma k} r_{\delta l} S_{ijkl}, \quad \ldots (1)$$

where Einstein's summation rule is adopted, $r_{\alpha i}$ is the component of the rotation matrix (or direction cosines). The transformation can be substantially simplified in the calculation of specific modulus. The uniaxial stress can be represented as a unit vector, and advantageously described by two angles (θ, φ); we choose it to be the first unit vector in the new basis set *a*. The determination of some elastic properties (shear modulus, Poisson's ratio) requires another unit vector *b*, perpendicular to unit vector *a*, and characterized by the angle χ. The coordinates of two vectors[30,31] are:

$$a = \begin{pmatrix} \sin\theta\cos\varphi \\ \sin\theta\sin\varphi \\ \cos\theta \end{pmatrix}$$

and

$$b = \begin{pmatrix} \cos\theta\cos\varphi\cos\chi - \sin\varphi\sin\chi \\ \cos\theta\sin\varphi\cos\chi + \cos\varphi\sin\chi \\ -\sin\theta\cos\chi \end{pmatrix}. \quad \ldots (2)$$

The Young's modulus can be obtained by using a purely normal stress in $\varepsilon_{ij} = S_{ijkl}\,\sigma_{kl}$ in its vectors form and it is given by:

$$E(\theta,\varphi) = \frac{1}{S'_{11}(\theta,\varphi)} = \frac{1}{r_{1i} r_{1j} r_{1k} r_{1l} S_{ijkl}} = \frac{1}{a_i a_j a_k a_l S_{ijkl}}. \quad \ldots (3)$$

Other properties depend on two directions (if perpendicular, this corresponds to 3 angles) and make them difficult to be represented graphically. A convenient possibility is to consider three representations: minimum, average and maximum. For each θ and φ, the angle χ is scanned and the minimum, average and maximum values are recorded for this direction. The definitions of angles used to describe directions in calculations are shown in Fig. 1. The shear modulus is obtained by applying a pure shear stress in the vector form and results in:

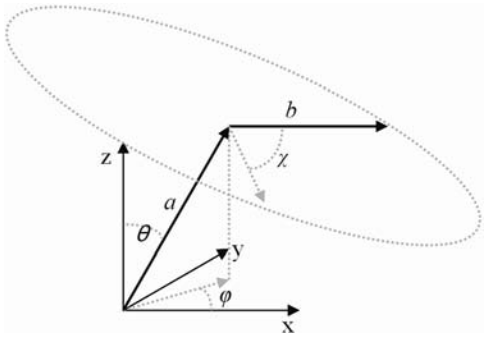

Fig. 1—Definitions of angles used to describe directions in calculations

Table 1—Lattice constants *a*, *c* (in Å), and cell volume per formula unit V_0 (in Å^3) for $P4_2$/mnm-BC

Crystal	method	*a*	*c*	*V*
BC	GGA[a]	4.401	2.766	6.696
	GGA[b]	4.376	2.759	6.610
	LDA[a]	4.314	2.723	6.334

[a]Present work, [b]Ref.[21]

$$G(\theta,\varphi,\chi)=\frac{1}{4S'_{66}(\theta,\varphi,\chi)}=\frac{1}{4r_{1i}r_{2j}r_{1k}r_{2l}S_{ijkl}}$$

$$=\frac{1}{4a_ib_ja_kb_lS_{ijkl}}, \quad \ldots (4)$$

The Poisson's ratio can be expressed as:

$$v(\theta,\varphi,\chi)$$

$$=-\frac{S'_{12}(\theta,\varphi,\chi)}{S'_{11}(\theta,\varphi)}=-\frac{r_{1i}r_{1j}r_{2k}r_{2l}S_{ijkl}}{r_{1i}r_{1j}r_{1k}r_{1l}S_{ijkl}}=-\frac{a_ia_jb_kb_lS_{ijkl}}{a_ia_ja_ka_lS_{ijkl}}. \quad \ldots (5)$$

3 Results and Discussion

3.1 Structural properties

Table 1 lists the calculated equilibrium lattice parameters within GGA and LDA method for $P4_2$/mnm-BC together with the previous results. From Table 1, it is seen that our calculated lattice parameters for $P4_2$/mnm-BC are in excellent agreement with previous studies[21]. It is clear that the predicted lattice constants within LDA method are smaller than those within GGA method as the usual case. For $P4_2$/mnm-BC, there is no available experimental result. However, our predicted lattice parameters using GGA and LDA agree well the previously reported values[21]. Figure 2 (a) shows the dependence of the equilibrium lattice parameters on pressure, where a_0, and c_0 are the equilibrium conventional lattice constants at ambient pressure. For $P4_2$/mnm-BC, it can be easily seen that the compressibility along *c*-axis is more difficult than along *a*-axis (*b*-axis). To compare the incompressibility of $P4_2$/mnm-BC, the volume compressions V/V_0 (where V_0 is the equilibrium primitive cell volume at ambient pressure) of c-BN and diamond as a function of pressure, are also shown in Fig. 2 (a). It is seen that the incompressibility of $P4_2$/mnm-BC is slightly smaller than that of diamond and c-BN.

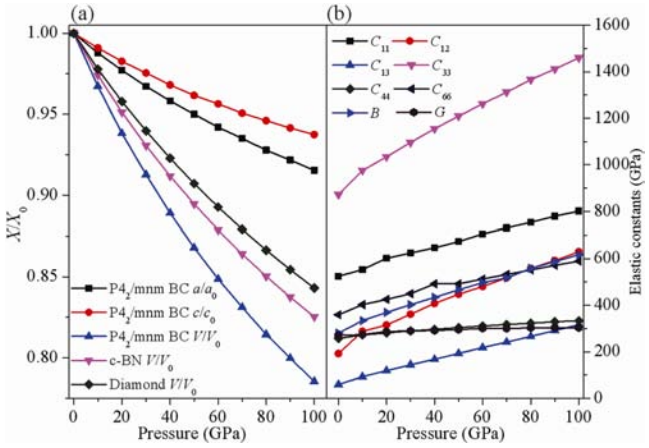

Fig. 2—(a) Lattice parameters a/a_0, and c/c_0 compression as functions of pressure for $P4_2$/mnm-BC, and primitive cell volume V/V_0 for $P4_2$/mnm-BC, c-BN, and diamond and (b) Elastic constants of $P4_2$/mnm-BC as a function of pressure

3.2 Elastic properties and anisotropic properties

The elastic properties give important information concerning the nature of the forces operating in solids. Particularly, they provide information about the stability and stiffness of materials. In the present paper, the elastic constants and elastic modulus of $P4_2$/mnm-BC, BC_7, BC_5, B_4C_4, and B_4C together with its previous results, which are presented in Table 2. For the tetrahedral $P4_2$/mnm-BC, six independent elastic constants C_{ij} (C_{11}, C_{12}, C_{13}, C_{33}, C_{44} and C_{66},) were obtained by introducing a small finite strain to equilibrium structure. The criteria for mechanical stability of tetragonal symmetry group[31] are given by: $C_{11} > 0$, $C_{33} > 0$, $C_{44} > 0$, $C_{66} > 0$, $C_{11} - C_{12} > 0$, $C_{11} + C_{33} - 2C_{13} > 0$, $2(C_{11} + C_{12}) + C_{33} + 4C_{13} > 0$

The calculated results show that the $P4_2$/mnm-BC is mechanically stable under ambient conditions. From Table 2, we noted that the elastic constants (C_{11}=524 GPa, C_{33}=873 GPa, C_{44}=257 GPa, C_{66}=359 GPa) of $P4_2$/mnm-BC are smaller[32] than B_4C_4

Table 2—Calculated elastic constant C_{ij} (GPa), bulk modulus B (GPa), shear modulus G (GPa), Young's modulus E (GPa), Poisson's ratio v and hardness of $P4_2$/mnm-BC, B_4C_4, B_4C, BC_7, and BC_5

	Method	C_{11}	C_{12}	C_{13}	C_{33}	C_{44}	C_{66}	B	G	E	v
BC	GGA[a]	524	192	59	873	257	359	280	270	613	0.14
	LDA[a]	542	269	83	954	271	408	321	276	644	0.17
	GGA[b]	502	263	74	919	244	297	302	254	595	0.17
B_4C_4[c]	GGA	656	191	167	562	311	382	324	285	660	0.16
B_4C[d]	GGA	491	88	92	534	204	192				
	LDA	512	100	105	561	208	197				
B_4C[e]	LDA	562	70	124	536		213				
BC_7[f]	GGA	769	196			498			399	891	0.12
	LDA	807	222			537			421	945	0.12
BC_5[f]	GGA	865	177	64	1086	382			386	865	0.12
	LDA	931	194	69	1164	401			410	922	0.13

[a]Present work, [b]Ref.[21], [c]Ref.[20], [d]Ref.[34], [e]Ref.[35], [f]Ref.[33]

(C_{11}=656 GPa, C_{33}=562 GPa, C_{44}=311 GPa, C_{66}=382 GPa)[20], BC_5 (C_{11}=791 GPa, C_{22}=798 GPa, C_{44}=472 GPa, C_{55}=445 GPa, C_{66}=472 GPa)[32], BC_7 (C_{11}=769 GPa, C_{44}=498 GPa)[33], and BC_5 (C_{11}=865 GPa, C_{33}=1086 GPa, C_{44}=382 GPa)[33], whereas slightly larger than B_4C [C_{11}=491 GPa, C_{33}=534 GPa, C_{44}=204 GPa, C_{66}=192 GPa[34]; C_{11}=562 GPa, C_{33}=536 GPa, C_{66}=213 GPa[35]. The elastic constants versus pressure for $P4_2$/mnm-BC are shown in Fig. 2 (b). All the elastic constants C_{ij} increase but with different rates under increasing pressure. C_{33} of $P4_2$/mnm-BC increases faster than others and C_{44} grows the slowest. The bulk modulus of $P4_2$/mnm-BC is the smallest in these boron-carbide compounds, so does the G. The Young's modulus E and Poisson's ratio v are taken[36] as: $E = 9BG/(3B+G)$, $v = (3B-2G)/[2(3B+G)]$. From Table 2, we noted that the bulk modulus of $P4_2$/mnm-BC (280 GPa) is smaller than[20] that of B_4C_4 (322 GPa). Poisson's ratio offers the fundamental metric to compare the performance of any material when strained elastically[37]. The Poisson's ratio v of $P4_2$/mnm-BC is 0.14 within GGA, slightly larger than other boron-carbide compounds, respectively. The calculated theoretical elastic modulus of $P4_2$/mnm-BC, and its Vickers hardness[21] (42 GPa), indicates that it is a potential superhard material.

Generally, the criterion proposed by Pugh[38] is adopted to estimate whether a crystalline solid is intrinsically ductile or brittle. The bulk modulus B represents the resistance to fracture, while the shear modulus G represents the resistance to plastic deformation. A higher B/G ratio is associated with ductility, whereas a lower value corresponds to brittle nature. If $B/G > 1.75$, the material behaves in a ductile manner; otherwise, the material behaves in a brittle manner. For tetrahedral $P4_2$/mnm-BC, the B/G value is 1.04 at 0 GPa. In this case, BC is prone to brittle. The B/G value increases monotonically with pressure. At 100 GPa, the B/G value is 2.04, suggesting a ductile manner. The brittle-ductile transition occurs at ~ 71 GPa.

Using Eqs (3-5), the calculated values of Poisson's ratio, shear modulus and Young's modulus along different directions as well as the projections in different planes are shown in Figs (3 and 4). In Fig. 3, the solid line represents maximum and dashed line represents minimum. We first focus on Poisson's ratio; Fig. 3 (a, b and c) shows the 2D representation of Poisson's ratio in the *xy*, *xz*, and *yz* planes for $P4_2$/mnm-BC, respectively. It is found that $0 \leq v \leq 0.36$, showing that v remains positive at 0 GPa. The minimum value at 0~100 GPa pressure range remains 0.0. The maximum value of Poisson's ratio at 50 GPa (100GPa) is 0.63 (1.07). The shear modulus for all possible directions of shear strain have also been calculated. The 2D representation of shear modulus in the *xy*, *xz*, and *yz* planes for $P4_2$/mnm-BC are shown in Fig. 3 (d, e and (f), respectively. It is observed that shear modulus varies between 166 and 363 GPa, the ratio G_{max}/G_{min}=2.19 and the average value of all directions is 268 GPa, which is close to the calculated result (270 GPa) using strain-stress method. Fig. 3 shows that the greater the pressure, the more obvious is the anisotropy.

We now focus on the Young's modulus. The directional dependence of the Young's modulus at different pressure, along the *xy*, *xz*, and *yz* planes for $P4_2$/mnm-BC are plotted in Fig. 4. It is clear that the

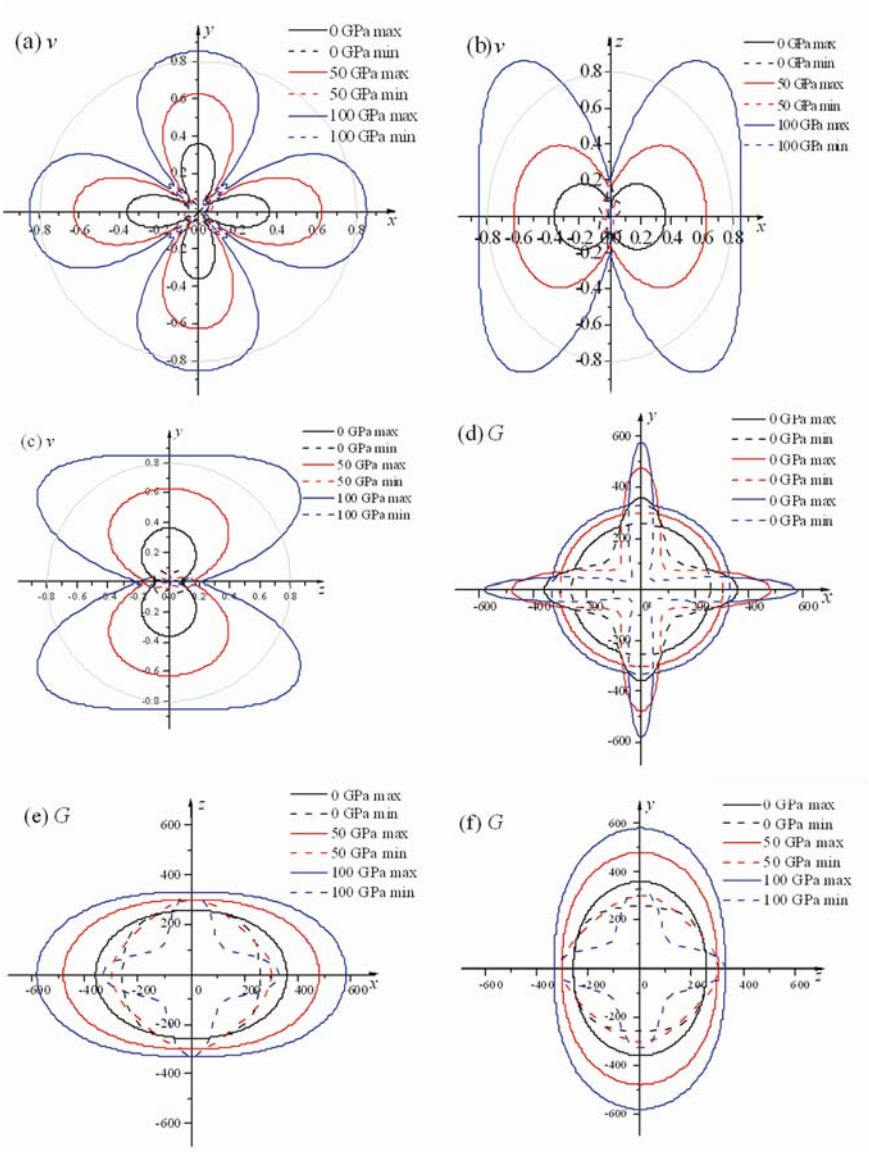

Fig. 3—2D representation of Poisson's ratio in the (a) *xy* plane, (b) *xz* plane and (c) *yz* plane for $P4_2/mnm$-BC. 2D representation of shear modulus in the (d) *xy* plane, (e) *xz* plane and (f) *yz* plane for $P4_2/mnm$-BC

Young's modulus for this material has large anisotropy, with a minimal value of E_{min}=452 GPa and a maximum of E_{max}=863 GPa. The average value in all directions is 577 GPa, the ratio E_{max}/E_{min}=1.91 at 0 GPa. The anisotropy increases quickly with increasing pressure. For example, the ratio E_{max}/E_{min} increases to 2.93 (6.89) at 50 (100) GPa.

3.3 Electronic properties

The calculated band structures and DOS of $P4_2/mnm$-BC at 0 GPa and 60 GPa are shown in Fig. 5. The Fermi level is set to 0 eV. It is known that the calculated band gap with DFT are usually underestimated by 30–50%, the true band gap must be larger than the calculated results. The main features of DOS for $P4_2/mnm$-BC at 0 GPa can be summarized as follows: (i) the peak present in the conduction band DOS (0 to 12.5 eV) of the DOS is mainly due to contributions of the *p* electrons of B, the contribution of the C atom is very small; (ii) the states from –12 eV to Fermi energy (0 eV) mainly originate from C-*p* orbital with less contributions of B-*p*, the contributions of the C atom *s* orbital and B atom *s* orbital are very small. (iii) The peak present in the energy part (-12 to -20 eV) of the DOS is mainly due to contributions of the *s* electrons of C atom and the contribution of the B atom *s* orbital is the smallest.

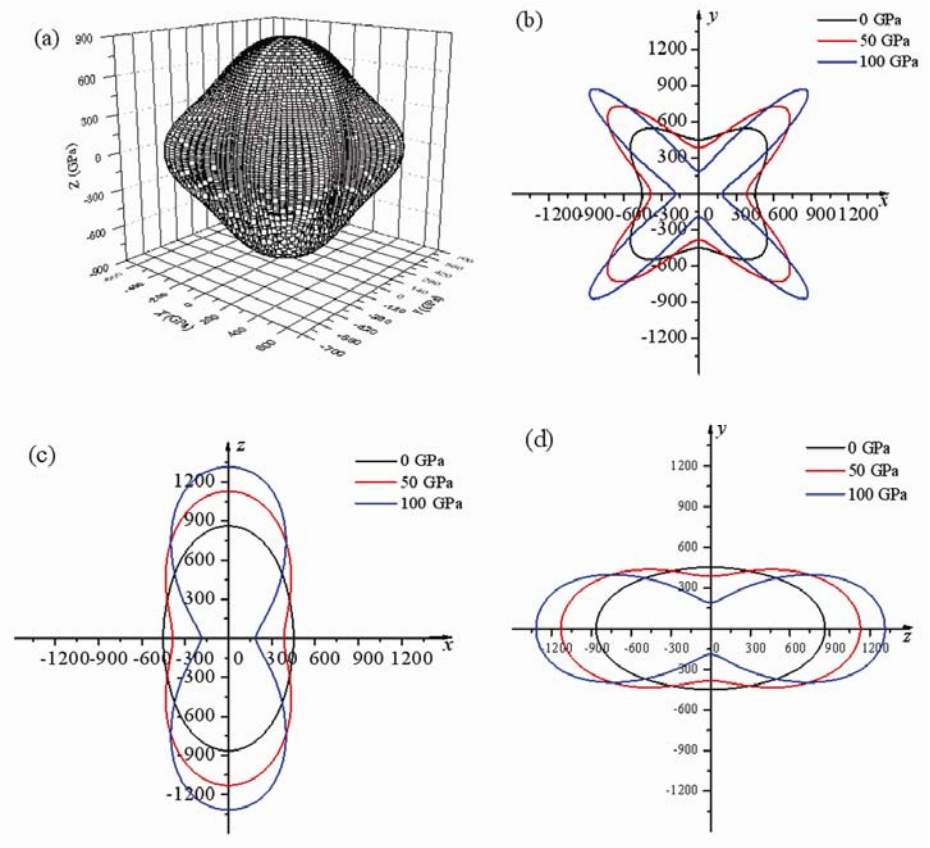

Fig. 4—(a) Directional dependence of the Young's modulus for $P4_2/mnm$-BC, 2D representation of Poisson's ratio in the (b) *xy* plane, (c) *xz* plane and (d) *yz* plane

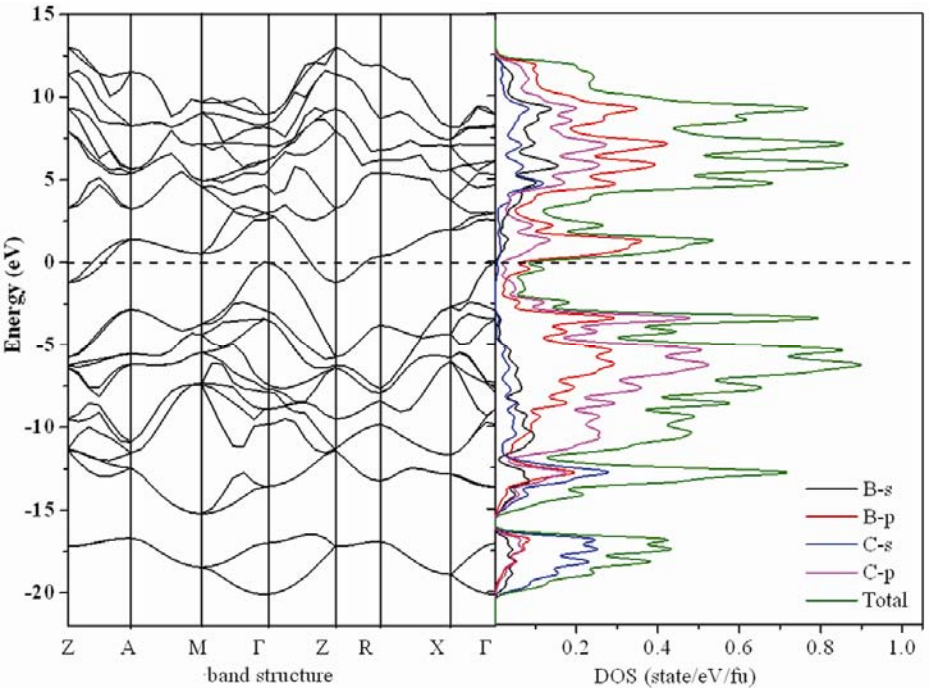

Fig. 5—Electronic band structure and density of state for the $P4_2/mnm$-BC at 0 GPa

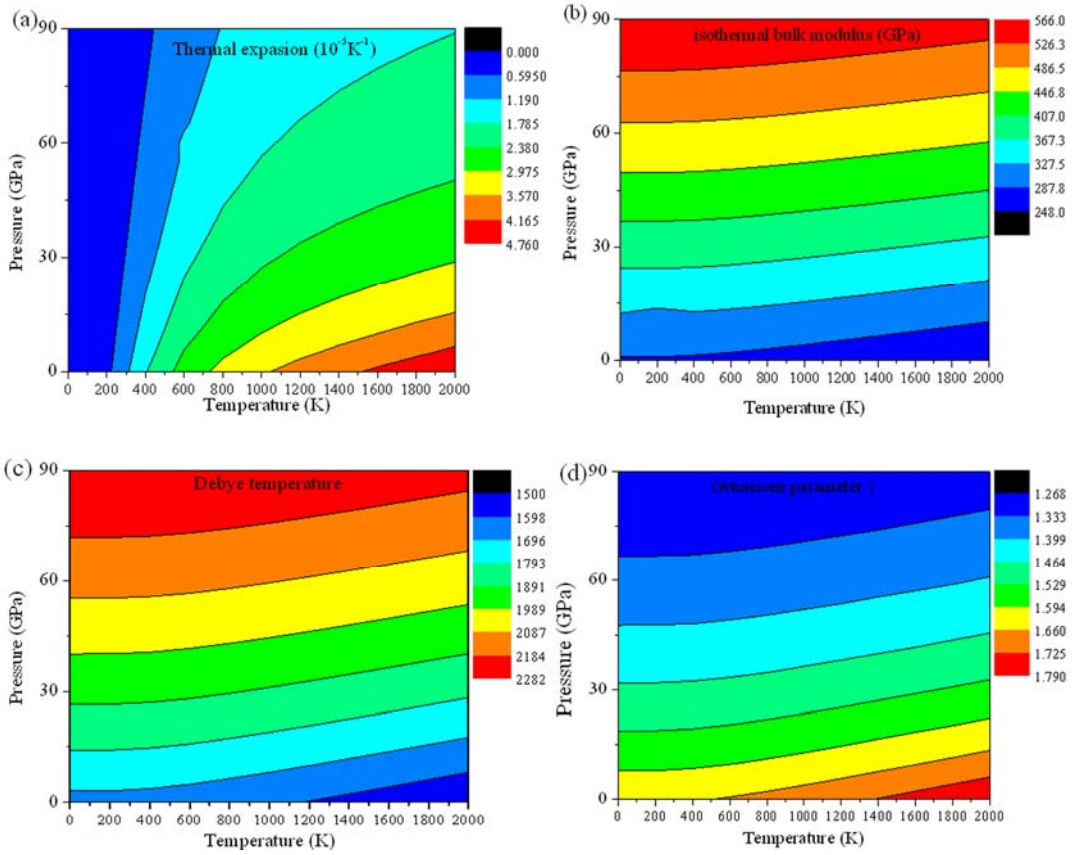

Fig. 6—(a)Two-dimensional contour plots of thermal expansion, (b) isothermal bulk modulus, (c) Debye temperature and (d) Grüneisen parameter versus pressure and temperature for $P4_2/mnm$-BC

3.4 Thermodynamic properties

In order to obtain the thermodynamic properties of $P4_2/mnm$-BC, the quasi-harmonic Debye model[39] was used in the present paper. The calculated relationships of thermal expansion, α, on pressure and temperature are shown in Fig. 6 (a). From Fig. 6 (a), with the increase in pressure, the thermal expansion coefficient α decreases, and the higher the temperature, the faster is the reduction in the thermal expansion coefficient α. The effects of pressure on α are small at low temperatures and increase with the increase in temperature. This is an indication of the inadequacy of the quasi-harmonic approximation at elevated temperatures and pressures. The isothermal bulk modulus B_S of $P4_2/mnm$-BC, as a function of pressure and temperature, is shown in Fig. 6 (b). Correspondingly, in Fig. 6 (b), when $T < 400$ K, the B_S of $P4_2/mnm$-BC has a little change; when $T > 400$ K, the B_S changes with increase in T. From Fig. 6 (b), it is found that the effect of temperature on B_S is not as significant as that of pressure in the calculated range of pressure and temperature.

The calculated relationships of Debye temperature Θ_D on pressure and temperature are plotted in Fig. 6 (c). The Θ_D is affected by both pressure and temperature. At a given temperature, the Θ_D increases quickly with increasing pressure. In other words, the Debye temperature decreases with temperature at certain pressure and increases with pressure at certain temperature. From Fig. 6 (c), the effect of temperature on the Debye temperature is less significant than that of pressure. The Grüneisen parameter, which describes the alteration in a crystal lattice vibration frequency, can reasonably predict the anharmonic properties of a solid, such as the temperature dependence of phonon frequencies and lattice volume. Usually, the Grüneisen parameter is positive and lies in the range 1.5±1.0. The calculated relationships of Grüneisen parameter γ with pressure and temperature are plotted in Fig. 6 (d). It is found that the Grüneisen parameter slightly increases with temperature at a given pressure, but decreases with pressure at a given temperature. At low temperature ($T < 600$ K), γ is constant, as well as slightly increases linearly with temperature at high temperature ($T > 600$ K). Fig. 6 (d)

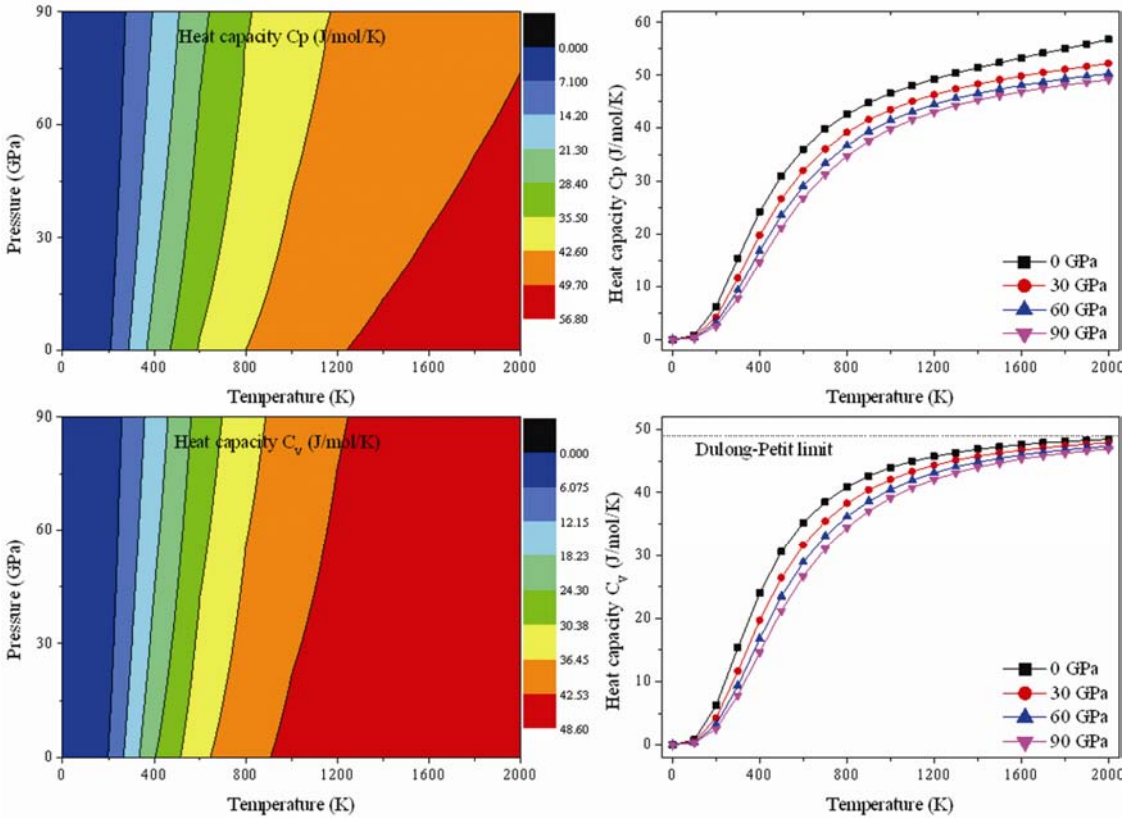

Fig. 7—Calculated specific pressure heat capacity C_P and volume heat capacity C_V as a function of pressure for $P4_2$/mnm-BC at different temperature: (a) C_P contours, (b) C_P-T, (c) C_V contours and (d) C_V-T

shows that the effect of the pressure on the Grüneisen parameter is more significant than that of temperature.

Figure 7 shows the two-dimensional contour plots of the dependence of heat capacity on pressure and temperature. The heat capacity in Debye model, which only contains these low frequency modes that are excited at low temperature, is an important measure of the thermodynamic properties. The difference between C_P and C_V is very small at low temperatures and low pressures. One can also see that the heat capacity (C_P and C_V) increases with temperature at the same pressure and decreases with pressure at the same temperature. The effect of temperature on heat capacity is much more significant than that of pressure. It also shows that, when $T <$ 1400 K, the heat capacity is sensitive to both temperature and pressure. At high temperature, the calculated heat capacity is expected to converge to a constant $3N_Ak_B \approx 49.85$ $Jmol^{-1}K^{-1}$ according to the law of Dulong and Petit.

4 Conclusions

The structural properties, elastic properties, elastic anisotropy, electronic properties, and thermodynamic properties of the $P4_2$/mnm-BC under high pressure, have been investigated by the First-principles calculations in combination with the quasi-harmonic Debye model. The elastic constants, elastic modulus under high pressure and high temperature, and the anisotropies of $P4_2$/mnm-BC are also calculated for the first time. By the elastic stability criteria, it is predicted that $P4_2$/mnm-BC is stable. In addition, the obtained B/G ratio indicates that $P4_2$/mnm-BC exhibits brittle to ductile transitions in the present studied pressure range. The $P4_2$/mnm-BC exhibits a large anisotropy in its Poisson's ratio, shear modulus and Young's modulus, and the elastic anisotropy increases quickly with increasing pressure. Band structure study shows that $P4_2$/mnm-BC is a conductor. Moreover, we predict the thermodynamic properties and obtain the relationships among the thermal expansion, temperature and pressure, as well as the variations in isothermal bulk modulus, Debye temperature, Grüneisen parameter and heat capacity.

Acknowledgement

This work was financially supported by the Fundamental Research Funds for the Central

Universities, Natural Science Foundation of China (No. 11204007), and Natural Science Basic Research plan in Shaanxi Province of China (grant No. 2013JQ1007). This work was supported by Shenzhen Supercomputer Center of China.

References

1 Calandra M & Mauri F, *Phys Rev Lett*, 101 (2008) 016401.
2 Solozhenko V L, Kurakevych O O, Andrault D, Godec Y Le & Mezouar M, *Phys Rev Lett*, 102 (2009) 015506.
3 Ekimov E A, Sidorov V A, Bauer E D, Melnik N N, Curro N J, Thompson J D & Stishov S M, *Nature*, 428 (2004) 542.
4 Blase X, Adessi Ch & Connétable D, *Phys Rev Lett*, 93 (2004) 237004.
5 Bustarret E, Kacmarcik J, Marcenat C, Gheeraert E, Cytermann C, Marcus J & Klein T, *Phys Rev Lett*, 93 (2004) 237005.
6 Yokoya T, Nakamura T, Matsushita T, Muro T, Takano Y, Nagao M, Takenouchi T, Kawarada H & Oguchi T, *Nature*, 438 (2005) 647.
7 Jones L E & Thrower P A, *Carbon*, 29 (1991) 251.
8 Xu L F, Zhao Z S, Wang L M, Xu B, J He L, Liu Z Y & Tian Y J, *J Phys Chem C*, 114 (2010) 22688.
9 Yang J, H Sun, He J L, Tian Y & Chen C F J, *J Phys Cond Matter*, 19 (2007) 346223.
10 Zinin P V, Ming L C, Ishii H A, Jia R & Acosta T, *J Appl Phys*, 111 (2012) 114905.
11 Shirasaki T, *Carbon*, 38 (2000) 1461.
12 Krishnan K M, *Appl Phys Lett*, 58 (1991) 1857.
13 Schwetz K A & Karduck P, *AIP Conf Proc*, 231 (1990) 405.
14 Bylander D M & Kleinman L, *Phys Rev B*, 42 (1990) 1394.
15 Bylander D M & Kleinman L, *Phys Rev B*, 43 (1991) 1487.
16 Kleinman L, *AIP Conf Proc*, 231 (1991) 13.
17 Schmechel R & Werheit H, *J Phys Condens Matter*, 11 (1999) 6803.
18 Schmechel R & Werheit H, *J Solid State Chem*, 154 (2000) 61.
19 Zhang Y F & Wang L, *J Phys Soc Jpn*, 82 (2013) 073702.
20 Zheng B, Zhang M G & Luo H G, *EPL*, 108 (2014) 16001.
21 D Y Wang, Q Yan, B Wang, Y X Wang, J M Yang & G Yang, *J Chem Phys*, 140 (2014) 224704.
22 Hohenberg P & Kohn W, *Phys Rev*, 136 (1964) 864.
23 Kohn W & Sham L J, *Phys Rev*, 140 (1965) 1133.
24 J Perdew P, Burke K & Ernzerhof M, *Phys Rev Lett*, 77 (1996) 3865.
25 D Ceperley M & Alder B J, *Phys Rev Lett*, 45 (1980) 566.
26 Perdew J P & Zunger A, *Phys Rev B*, 23 (1981) 5048.
27 Clark S J, Segall M D, Pickard C J, Hasnip P J, Probert M I J, Refson K & Payne M C, *Z Kristallogr*, 220 (2005) 567.
28 Monkhorst H J & Pack J D, *Phys Rev B*, 13 (1976) 5188.
29 Pfrommer B G, Côté M, Louie S G & M Cohen L, *J Comput Phys*, 131 (1997) 233.
30 Marmier A, Lethbridge Z A D, Walton R I, Smith C W, Parker S C & Evans K E, *Comput Phys Commun*, 181 (2010) 2102.
31 Watt J P & Peselnick L, *J Appl Phys*, 51 (1980) 1525.
32 Li M M, Fan X F & Zheng W T, *J Phys: Condens Matter*, 25 (2013) 425502.
33 Zhang Q, Wang S M & Liang Y C, Zhejiang Univ-Sci A, *Appl Phys Eng*, 12, (2011) 177.
34 Jay A, Vast N, Sjakste J & Duparc O H, *Appl Phys Lett*, 105 (2014) 031914.
35 Lee S, D Bylander & Kleinman L, *Phys Rev B*, 45 (1992) 3245.
36 Fan Q Y, Wei Q, Yan H Y, M Zhang G, Zhang Z X, Zhang J Q & Zhang D Y, *Comput Mater Sci*, 85 (2014) 80.
37 Greaves G N, Greer A L, Lakes R S & Rouxel T, *Nature Mater*, 10 (2011) 823.
38 Pugh S F, *Philos Mag*, 45 (1954) 823.
39 Blanco M A, Francisco E & Luaña V, *Comput Phys Commun*, 158 (2004) 57.